RSC Advances

PAPER

View Article Online
View Journal | View Issue

Cite this: *RSC Adv.*, 2023, **13**, 26111

Evaluation of dual potentiality of 2,4,5-trisubstituted oxazole derivatives as aquaporin-4 inhibitors and anti-inflammatory agents in lung cells†

Maniarasu Meenakshi,[a] Arun Kannan,[b] Muralidharan Jothimani,[c] Thangavel Selvi,[a] Muthusamy Karthikeyan,[c] Chidambaram Prahalathan*[b] and Kannupal Srinivasan*[a]

Received 14th June 2023
Accepted 15th August 2023

DOI: 10.1039/d3ra03989g

rsc.li/rsc-advances

Inflammation is a multifaceted "second-line" adaptive defense mechanism triggered by exo/endogenous threating stimuli and inter-communicated by various inflammatory key players. Unresolved or dysregulated inflammation in lungs results in manifestation of diseases and leads to irreparable damage. Aquaporins (AQPs) are a ubiquitously expressed superfamily of intrinsic transmembrane water channel proteins that modulate the fluid homeostasis. In addition to their conventional functions, AQPs have clinical relevance to inflammation prevailing under the infectious conditions of various lung diseases and this proclaims them as appropriate biomarkers to be targeted. Hence an endeavor was undertaken to identify potential ligands to target AQP4 for the treatment of lung diseases. Oxazole being a versatile bio-potent core, a series of 2,4,5-trisubstituted oxazoles **3a–j** were synthesized by a Lewis acid mediated reaction of aroylmethylidene malonates with nitriles. *In silico* studies conducted using the protein data bank (PDB) structure 3gd8 for AQP4 revealed that compound **3a** would serve as a suitable candidate to inhibit AQP4 in human lung cells (NCI-H460). Further, *in vitro* studies demonstrated that compound **3a** could effectively inhibit AQP4 and inflammatory cytokines in lung cells and hence it may be considered as a viable drug candidate for the treatment of various lung diseases.

Introduction

Inflammation is a complex and dynamic surveillance mechanism which responds to various noxious stimuli. This crucial mechanism involves multiple inflammatory players including pro-inflammatory cytokines (like TNFα, IFNγ, IL-1β, IL-6 and IL-2), chemokines, adhesion molecules and anti-inflammatory factors (such as TGF-β, IL-4, IL-10 and IL-13), which have a profound impact both at cellular and molecular levels.[1] Conversely to its protective role, any failures in feedback inhibition mechanisms are responsible for the attenuation of the process leading to excessive inflammatory cell recruitment. The induction of a "cytokine storm" is known to be a hallmark of various lung diseases including influenza A virus (IAV) infection and Covid-19.[2] The exaggerated inflammatory state provoked by hypercytokinemia engenders alveolar damage, acute respiratory distress (ARDS), and pulmonary edema leading to severe comorbidity and mortality.[3] Alleviation of the hyper-inflammatory state and fluid clearance remain significant protocols to improve the prognosis of lung diseases.

Aquaporins (AQPs) – "the plumbing system for cells" constitute a large family of membrane water channel proteins (WCPs), which play a vital role in regulation of water fluid homeostasis in response to osmotic gradients. There are 13 prevalent isoforms of AQPs, AQP0–AQP12 and they are quite ubiquitous in diverse mammalian cells. On the basis of function and phylogenesis, this super family of WCPs are sub-categorized into (i) "orthodox" which are confined only to transportation of water (AQP0, AQP1, AQP2, AQP4, AQP5), (ii) "aquaglyceroporins" which are permeable to water and other small non-polar molecules like glycerol (AQP3, AQP7, AQP9, AQP10) (iii) "superaquaporins" which can transport certain charged and neutral solutes (AQP6, AQP8, AQP11, AQP12).[4] In addition to their secretive and absorptive functions, AQPs also mediate other physiological processes such as cell migration, cell proliferation, adipocyte metabolism, neuro excitation *etc.*[5] Extensive data indicate that AQPs play a prominent role in several pathological conditions like intestinal bowel disease

[a]*School of Chemistry, Bharathidasan University, Tiruchirappalli-620024, Tamil Nadu, India. E-mail: srinivasank@bdu.ac.in*

[b]*Department of Biochemistry, Bharathidasan University, Tiruchirappalli-620024, Tamil Nadu, India*

[c]*Department of Bioinformatics, Alagappa University, Karaikudi-630003, Tamil Nadu, India*

† Electronic supplementary information (ESI) available: Copies of ^{1}H and ^{13}C NMR spectra of all products. See DOI: https://doi.org/10.1039/d3ra03989g

(IDB),[6] cerebral edema,[7] neuroinflammation[8] and hypoxia.[9] Amongst various isoforms, AQP1, AQP3, AQP4 and AQP5 are expressed in lungs and regulate cell function *via* transcellular pathway of water across the lung microvascular endothelium and epithelia.[10] Though the underlying signaling pathways and molecular mechanisms driving osmotic stress-induced inflammatory response still remain untangled, the pertinence of AQPs to inflammation during the onset of various lung diseases like asthma, pneumonia, pulmonary edema, bronchitis and Covid-19 are well documented.[11] Thus it comes to light that AQPs participate in pathophysiological processes apart from their conventional activity of fluid trafficking between inter cellular spaces and this makes them suitable biomarkers to be targeted for the diagnosis and/or treatment of various inflammatory diseases.[12] Studies on various models of lung inflammation show the differential regulation of all the four isoforms of AQPs that are expressed in lungs. Recent factual evidence shows that AQP4 is found to be upregulated in numerous inflammatory conditions of lung diseases.[13] Drugs which target AQPs are anticipated to possess a wide spectrum of pharmacological applications because of the ubiquitous nature and pathophysiological implication of AQP in inflammation. Recent advancement in the discovery of drugs for AQP and future orientation towards the identification of appropriate AQP inhibitors were well documented.[14–16]

AQP inhibitors like tetraethylammonium (TEA) interacts with tyrosine residues at pore-lining thereby inhibits water permeability reversibly and selectively through AQP1, AQP2 and AQP4.[17,18] Acetazolamide, a first generation carbonic anhydrase inhibitor which is primarily used for the treatment of glaucoma is found to inhibit AQP1 and AQP4 in *Xenopus* oocytes.[19] Other drugs like TGN-020, phloretin, bumetanide have drawn considerable attraction as potential AQP inhibitors.[14,20] Although several other putative small molecule aquaporin inhibitors were reported and patented for therapeutic usage, their lack of selectivity and toxic side effects impede their application in clinical trials.[14]

Non-steroidal anti-inflammatory drugs (NSAIDs) are extensively used for symptomatic relief by controlling pain, fever and inflammation in infected patients. Commercially available drugs like ibuprofen and naproxen continue to be the choice of drugs for treating lung inflammation.[21] Also, heterocyclic compounds such as oxazoles, thiazoles and imidazoles have been accredited for their anti-inflammatory potential. Especially, oxazole is a significant structural motif found in many natural products[22] and several oxazole derivatives exhibit a wide range of biological activities including anti-inflammatory, antibacterial, antifungal, antiviral, antitubercular, anticancer, antidepressant and neuroprotective activities.[23] Despite their wide spectrum of biological activities, the therapeutic efficacy of oxazoles as anti-inflammatory drugs through inhibition of AQP4 has not yet been reported to the best of our knowledge. Further, lack of appropriate drugs to downregulate the AQP4 expression opens up opportunities for the research community to develop new pharmacological therapies through modulation of AQPs. In the present study, we have synthesized a series of 2,4,5-trisubstituted oxazole derivatives and investigated their ability to modulate the expressions of AQP4 and inflammatory cytokines.

Results and discussion

Chemistry

Aroylmethylidene malonates are versatile building blocks in organic synthesis for the access of various heterocyclic compounds.[24] They could be easily prepared by the oxidative condensation of commercially available aryl methyl ketones with diethyl malonate in the presence of iodine and cupric oxide in DMSO.[25] Aroylmethylidene malonates when treated with nitriles in the presence of tin(IV) chloride undergo conjugate addition followed by ring closure to give oxazoles in 72–92% yields (Table 1).[24b] The synthesized compounds **3a–j** were characterized by IR, NMR and HRMS techniques. The IR spectrum of **3a** displayed absorbances at 2982, 1735, 1581, 1446, 1372, 1296, 1238, 1148, 1028, 942, 780, 688 and 595 cm^{-1}. The ^1H NMR spectrum of **3a** showed a six-proton triplet at δ 1.26 for the two ester methyl protons, a three-proton singlet at δ 2.54 for methyl protons attached to the oxazole ring, a four-proton multiplet at δ 4.22–4.28 for two ester methylene protons and a one-proton singlet at δ 4.88 for malonate methine proton in addition to five aromatic protons in the region of δ 7.39–7.57. In the ^{13}C NMR spectrum of **3a**, the two ester methyl carbons appeared at δ 13.9, the methyl carbon attached to the oxazole ring at δ 14.1, malonate methine carbon δ 50.7, the two ester

Table 1 Synthesis of oxazoles[a]

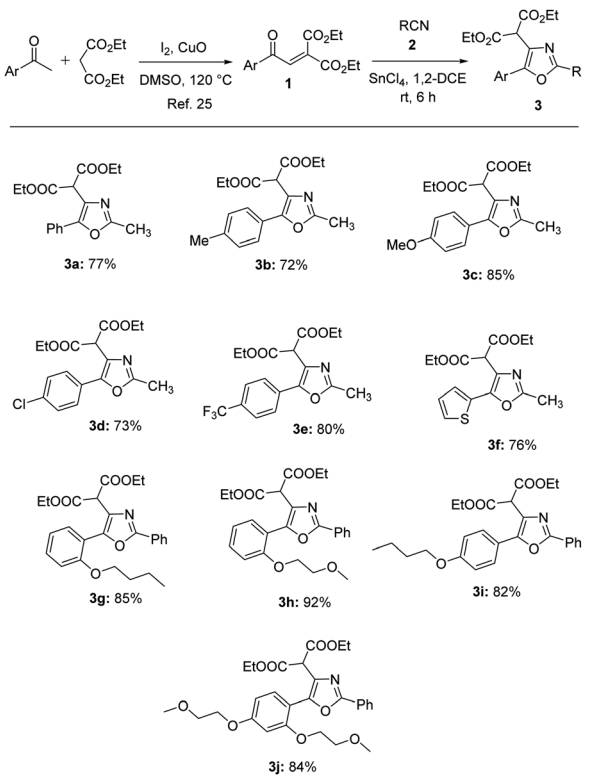

[a] Isolated yield.

methylene carbons at δ 62.1 and the two ester carbonyl carbons at δ 166.9 in addition to seven aromatic carbons in the region of δ 126.4–160.3. Similar NMR patterns were observed for other oxazole derivatives **3b–j**. The HRMS spectra of the tri-substituted oxazoles displayed peaks corresponding to the $[M + H]^+$ ion.

In silico analysis on aquaporin-4 inhibition

We employed a combination of computational methods to examine the intracellular inhibition of AQP4 by 2,4,5-trisubstituted oxazoles **3a–j**. Using AutodockVinasoftware, putative binding sites on the putative binding sites on the AQP4 subunit for the compounds were proposed based on molecular modeling and docking (Fig. 1 and Table 2). All the studied compounds showed good binding scores and they have a binding energy in the range of −6.1 to −7.3 kcal mol^{-1}, with compound **3a** having the highest binding energy of −7.3 kcal mol^{-1}. The binding energy was calculated based on the hydrophobic side chain interaction and specific energy that contributes to the molecule binding. Out of curiosity, we performed structure activity relationship studies on hypothetical oxazoles **3k–l** by replacing the R group of the oxazole ring by –CF_3/–Et group and also the diester group by mono/di carboxylic acid/amide group (see Table 1 in ESI†). To our surprise, the *in silico* analysis revealed that compound **3a** had a better binding affinity towards AQP4 protein when compared to all the other synthetic and hypothetical oxazole derivatives.

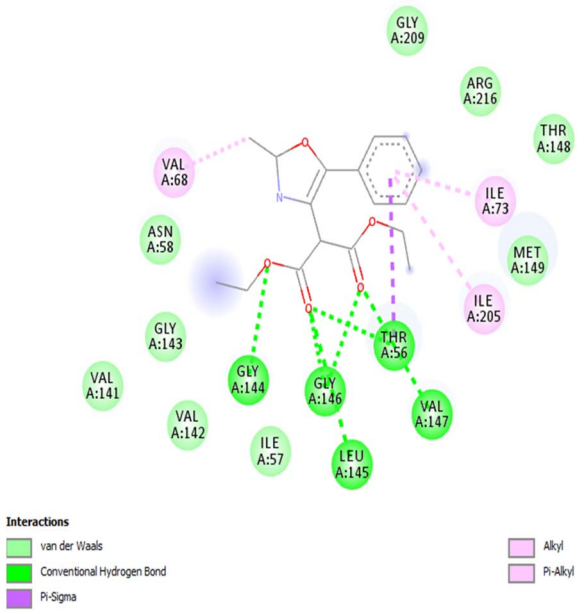

Fig. 1 2D image of interactions between AQP4 and oxazole **3a**.

ADME prediction

In silico prediction of ADME (absorption, distribution, metabolism and excretion) properties is essential to predict the biological effect of the molecules, before taking them into the experimental testing. So, the ADME properties of oxazoles **3a–j** were predicted using the QikProp module of the Schrodinger suite. The drug-likeness descriptors such as molecular weight, Qplogpo/w, QplogBB, QPPMDCK, QPPCaCo and percentage human oral absorption based on Lipinski's rule of five are given in Table 3. The QplogPo/w is the partial coefficient factor which examines crucial intake of absorption and estimation inside the body. The values of QplogPo/w range from 3.1 to 6.0 for the screened oxazole derivatives **3a–j**. The cell permeability factor QPPCaco determines the metabolism reaction of the drug inside the body condition and the values range from 1401 to 2002 for **3a–j**. Except for **3j**, the human oral absorption for all other oxazoles was estimated to be 100%. The compounds also satisfy the Lipinski's rule of 5. Thus, the ADME results show that the oxazoles **3a–j** have pharmacokinetic features within the acceptable range and potentially possess a drug-likeness nature for human use.

In vitro analysis on AQP4 inhibition

For *in vitro* studies, we selected oxazole **3a** as a representative compound as it had the highest binding energy with AQP4. The dose-dependent effect of lipopolysaccharide (LPS) and compound **3a** on cell viability in NCI-H460 cells were analyzed using MTT assay. In the present study, NCI-H460 cells were treated with different concentrations of LPS for 48 h and IC50 value at 30 μg showed 50% decrease in cell viability (Fig. 2A). Further, NCI-H460 cells treated with oxazole **3a** at different concentrations for 24 h significantly decreased the cell viability

Table 2 Docking score of oxazoles **3a–j**

S. no.	Compound	Binding energy (kcal mol^{-1})	Interacting residues
1	**3a**	−7.3	GLY144, GLY146, ILE73, ILE205, LEU145, THR56, VAL68, VAL147
2	**3b**	−6.1	HIS201, ILE57, ILE73, ILE205, THR56
3	**3c**	−6.5	ARG216, GLY209, HIS201, ILE57, ILE73, ILE205, MET149, PHE77, THR56
4	**3d**	−6.3	ARG216, GLY209, HIS201, ILE57, ILE73, ILE205, MET149, THR56
5	**3e**	−6.9	ARG216, ASN206, HIS201, GLY209, ILE57, ILE73, ILE205, MET149, PHE77, THR56, VAL150
6	**3f**	−6.2	ALA176, ALA192, ARG182, ILE189, PHE172, THR173, VAL185
7	**3g**	−6.6	GLY143, GLY144, GLY146, ILE73, ILE205, MET149, THR56, VAL147, VAL68
8	**3h**	−6.8	GLY146, ILE73, ILE205, THR56, VAL147, VAL68
9	**3i**	−6.5	ALA176, ALA192, ARG182, LEU191, PHE172, PHE195
10	**3j**	−7.1	ASN58, ASP69, ASN206, ARG216, GLY144, GLY209, VAL68

Table 3 Physicochemical properties calculated for oxazoles **3a–j** using Qikpro

Compound	Molecular weight (g mol^{-1})	QPlogS	QPlogHERG	QPPCaco	QPPMDCK	QPlogKp	QPlogPo/w	Human oral absorption	Rule of five
3a	317.341	−4.244	−5.504	1583.218	812.886	−1.901	3.156	100	0
3b	331.368	−4.965	−5.527	1401.242	712.383	−2.199	3.453	100	0
3c	347.367	−4.367	−5.385	1606.292	825.7	−1.989	3.215	100	0
3d	351.786	−5.06	−5.474	1579.846	1999.186	−2.061	3.671	100	0
3e	385.339	−5.754	−5.498	1593.481	3607.933	−2.123	4.165	100	0
3f	323.363	−3.892	−5.107	1759.474	1241.048	−1.951	2.992	100	0
3g	451.518	−7.156	−6.945	1972.184	1030.75	−0.897	5.768	100	1
3h	453.491	−6.028	−6.91	1793.371	930.117	−0.965	4.753	100	0
3i	451.518	−8.102	−7.531	2002.569	1047.926	−0.836	6.004	100	1
3j	527.57	−6.335	−7.094	1845.361	959.296	−0.761	5.002	88.772	2

at IC50 concentration of 60 μM (Fig. 2B). We therefore treated NCI-H460 cells with LPS at 30 μg for 48 h and compound **3a** at 60 μM for 24 h for all the subsequent experiments.

The free hemoglobin in plasma may cause damage to vital organs, such as heart, kidney, and liver. Hence, it is essential to investigate the hemolytic activity of biologically active compounds. So, *in vitro* hemolysis assay was carried out as a preclusive test for assessing the toxicity of compound **3a**. The hemoglobin produced as a result of membrane disruption upon treatment with **3a** was assessed. Accordingly, the hemocompatibility of **3a** was evaluated against human RBC. As shown in Fig. 2C, the compound **3a** was tested at different concentrations (60 μM, 300 μM and 600 μM). The hemolytic activity was found to be 1.5% for 60 μM (IC50 concentration), 1.6% for 300 μM (5 times greater than IC50) and 1.6% for 600 μM (10 times greater than IC50). The value is near to the one obtained by using phosphate-buffered saline (PBS) (negative control). On the other hand 0.1% Triton X-100 (positive control) treated group displays 100% hemolysis. According to ISO/TR 7406, samples with a hemolytic rate of less than 5% (the critical safe hemolytic ratio for biomaterials) are considered non-hemolytic. Hence, compound **3a** possesses a good blood compatibility without the cell membrane-disrupting activity.

AQP4 is one of the key players in edema formation and resolution. AQP4 is expressed in the ciliated columnar cells of various epithelial regions (nasopharyngeal, tracheal, bronchial) in the upper airways. Several processes including airway hydration, alveolar transport and submucosal gland secretion are mediated by water transport across epithelia and endothelia in the peripheral lung. In the present study, inflammation was induced in NCI-H460 cells by treating with 30 μg of LPS and the effect of LPS on AQP4 gene and protein expressions were studied. Our results indicated that AQP4 m-RNA expression was significantly upregulated (7-fold) on LPS treatment as shown in the Fig. 2D. Furthermore, we investigated the protein expression of AQP4 under LPS treatment and was found to be significantly increased compared to controls as shown in Fig. 2E. Thus, the results confirmed that AQP4 expression was increased under inflammation in NCI-H460 cells. It has been shown earlier that increased expression of AQP4 upregulates cytokine expression under inflammation. Thus, we examined the effect of compound **3a** on cytokine expressions in NCI-H460 cells. Accordingly, NCI-H460 cells were treated with LPS, compound **3a** and also LPS pretreated with compound **3a** and the cytokine expressions of cyclooxygenase-2 (COX-2), TNF-α, IL-1β, IL-6, IL-8 and IL-10 were studied using real time PCR (qRT-PCR). The m-RNA expression of the cytokines COX-2, TNF-α, IL-1β, IL-6, IL-8, IL-10 were significantly increased on LPS treatment. NCI-H460 cells treated with compound **3a** and LPS pre-treated with compound **3a** significantly downregulated the gene expressions for the cytokines COX-2, TNF-α, IL-1β, IL-6, IL-8, IL-10 as compared to LPS treated groups as shown in the Fig. 2F. Overall results indicated that increased expression of AQP4 increased cytokine expressions and pre-treatment or treatment with compound **3a** in turn decreased these cytokines under inflammation.

To envisage the effect of compound **3a** on AQP4 expression, we studied gene expression of AQP4 on NCI-H460 cells treated with LPS, compound **3a** and also LPS pretreated with compound **3a** by using qRT-PCR. Our results demonstrated that LPS significantly increased AQP4 expression and surprisingly, on compound **3a** treatment and pre-treatment significantly down-regulated AQP4 m-RNA expression as shown in the Fig. 2G. Further, the same was confirmed analyzing the protein expressions of COX-2 and AQP4 on NCI-H460 cells treated with compound **3a** and pre-treatment. As shown in Fig. 2H, LPS drastically increased the protein expressions of AQP4 and COX-2, but compound **3a** treatment and pre-treatment significantly decreased the expressions of the same. Thus, our data suggest that compound **3a** inhibits the expression of AQP4 and thus decreases the expressions of cytokines under inflammation in NCI-H460 cells.

Inflammation is a complex protective mechanism which provoke against any offending agent. Imbalanced inflammatory response leads to amplification of cytokines production, which in turn leads to organ damage. AQPs which are primarily known for their standard functionality of mediating transcellular fluid across the cell. Although several studies have demonstrated the differential regulation of AQP1, AQP3, AQP4 and AQP5 in various inflammatory models,[26] AQP4 is specifically found to be constantly upregulated during inflammatory condition. Liu *et al.* have demonstrated that AQP4 elevates brain edema by

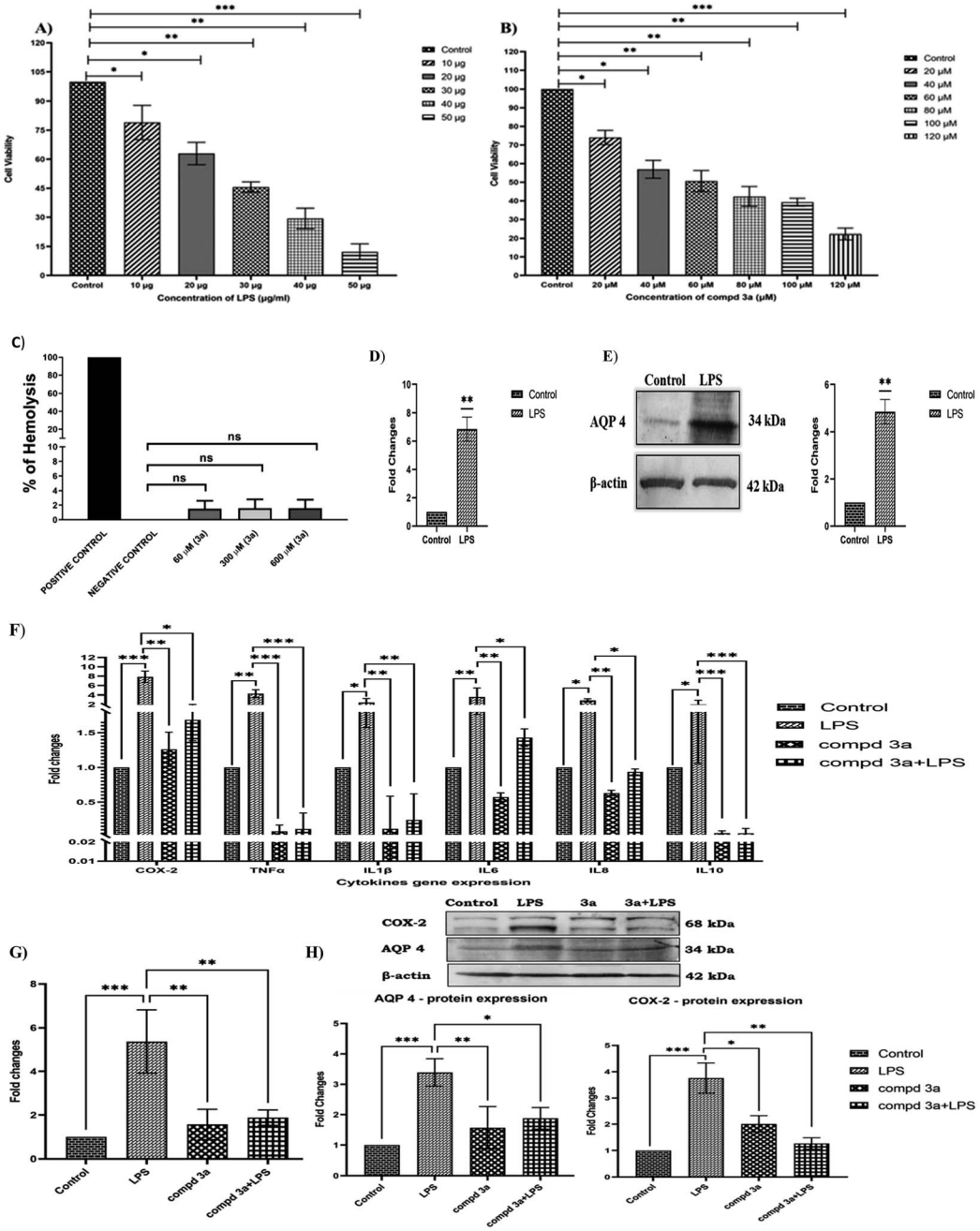

Fig. 2 (A) NCI-H460 cells were treated with different concentrations of LPS for 48 h and cell viability was determined by MTT assay; (B) NCI-H460 cells were treated with **3a** at different concentrations for 24 h and IC50 value was found to be 60 μM; (C) effect of **3a** at different concentrations (60 μM, 300 μM and 600 μM) on RBC hemolysis. (D) and (E) Effect of LPS on AQP4 gene and protein expression on NCI-H460 cells treated with 30 μg of LPS for 48 h were studied using real time PCR (qRT-PCR) and western blotting; (F) differential expression of cytokines in NCI-H460 cells control (untreated), LPS treated (30 μg, 48 h), **3a** treated (60 μM, 24 h) and LPS (30 μg, 48 h) pre-treated with **3a** (60 μM, 24 h) groups using real time PCR (q-RTPCR); (G) effect of LPS and **3a** in AQP4 gene expression in NCI-H460 cells control (untreated), LPS treated (30 μg, 48 h), **3a** treated (60 μM, 24 h) and LPS (30 μg, 48 h) pre-treated with **3a** (60 μM, 24 h) groups using real time PCR (q-RTPCR); (H) differential expression of AQP4 and COX-2 protein in NCI-H460 cells treated with LPS (30 μg, 48 h), **3a** (60 μM, 24 h), and LPS (30 μg, 48 h) pre-treated with **3a** (60 μM, 24 h) using western blotting. All the results were normalized with β-actin as an internal control. Values represent mean ± S.D. for three different experiments. Values are statistically significant at $*P < 0.05$, $**P < 0.01$, $***P < 0.001$.

increasing the water transfer into astrocyte during hypoxia ischemia (HI) and the downregulation of the AQP4 induces the anti-inflammatory response thereby helps in restoration of normal cerebral condition. Moreover, by silencing the AQP4, the expression of pro-inflammatory cytokines TNF-α, IL-1β and IL-10 were found to decrease.[27] Studies by Li *et al.* disclosed the pro-inflammatory role of AQP4 in experimental autoimmune encephalomyelitis (EAE). Intracerebral injection of LPS induced

greater neuroinflammation in wild-type than in AQP4-knockout mice. Astrocyte culture from AQP4-knock out mice showed reduced expression of cytokines. The result suggest that the reduction in AQP4 expression plays a protective role in neuroinflammatory CNS diseases by inhibiting water transport.[28] Further, Dai and his co-workers elucidated that AQP4 knockout led to the inhibition of mitogen-activated protein kinase (MAPK)/protein kinase B (AKT) pathway and alleviates the fluctuation of sphingosine kinase 1 (SPHK1) which eventually leads to decrease in cytokine secretion. The results of the experiments carried out in two genotypes, $AQP4^{+/+}$ and $AQP4^{-/-}$ exhibit increased production of TNF-α, IL-6 in LPS treated astrocytes. But significant low level of expressions of the same could be observed in $AQP4^{-/-}$. It is evident from the results that AQP4 deficiency alleviates the release of proinflammatory cytokines from astrocytes in association with SPHK1/MAPK/AKT pathway and underlines the role of AQP4 in neuroinflammation.[29] AQP4 deletion under insulin-induced hypoglycemic condition in mice was shown to exhibit positive neurological effect by attenuation of inflammatory response release (TNF-α, IL-6 and IL-1β) through the upregulation of PPAR-γ (peroxisome proliferator-activated receptor γ) and reduced brain edema thereby establishing blood–brain barrier (BBB) integrity.[30] The participation of AQP4 in modulation of seizure activity was clear from the outcome of studies by Binder *et al.* The seizure activity was monitored after the administration of chemoconvulsant pentylenetetrazol (PTZ) and the $AQP4^{-/-}$ mice did not exhibit seizure activity. AQP4 deficient mice showed decreased cerebral edema and improved neurological outcome in comparison with wild-type control.[31]

Among various heterocyclic compounds, oxazole scaffolds were reported to have valuable therapeutic applications because of their profound anti-inflammatory activity. Dunder *et al.*, have synthesized a series of 4,5-diphenyloxazolone derivatives and evaluated their COX-2 inhibitory potential. Among them, 4-(4-phenyl-3-methyl-2-oxo-3*H*-1,3-oxazol-5-yl)benzensulfonamide was found to possess the highest selective COX-2 inhibition.[32] Chobanian *et al.*, have identified a tri-substituted oxazole derivative, MK-4409 as potential selective fatty acid amide hydrolase (FAAH) inhibitor. *In vivo* studies showed that MK-4409 had excellent efficacy in various rodent inflammatory and neuropathic pain assays.[33] Seth *et al.* have reported 2-(2-arylphenyl)benzoxzole motifs as selective inhibitors of COX-2 with *in vivo* anti-inflammatory potential better than the standard drugs like diclofenac and celecoxib.[34] The compound **3a** used in the present study was also found to possess significant anti-inflammatory activity.

Conclusion

A series of highly substituted oxazole derivatives were prepared from aroylmethylidene malonates and nitriles through a conjugate addition followed by cyclization. The *in silico* analysis revealed that the synthesized compounds possess good AQP4 inhibitory activity and acceptable ADME properties. The *in vitro* studies performed taking oxazole **3a** as a representative compound demonstrated that it effectively inhibits the expression of AQP4 and cytokines and thus would serve as an appropriate drug candidate to reduce edema and suppress cytokines. The study opens up new scenarios in pharmacological therapies for treating various lung diseases including Covid-19.

Experimental section

General remarks

Melting points were determined by the open capillary tube method and were uncorrected. ^{1}H and ^{13}C NMR spectra were recorded on a 400 MHz NMR spectrometer. High-resolution mass spectra (ESI) were recorded on Q-TOF mass spectrometer. Thin layer chromatography (TLC) was performed on precoated alumina sheets and detection was done under UV light. Silica gel (100–200 mesh) was used for column chromatography.

Synthesis of oxazoles 3a–j

To a mixture of aroylmethylidene malonate **1** (ref. 25) (1 mmol) and nitriles **2** (1 mmol) in 1,2-dichloroethane (5 mL) was added $SnCl_4$ (1 mmol). The reaction mixture was stirred at room temperature for 6 h. After the reaction was complete, the reaction mixture was quenched with ice-water and extracted with dichloromethane. The organic layer was washed with water, dried (anhydrous Na_2SO_4) and the solvent was removed under reduced pressure. The crude product was purified by column chromatography using ethyl acetate/hexane to give pure oxazole **3**.

Diethyl 2-(2-methyl-5-phenyloxazol-4-yl)malonate (3a).[24b] Yellow oil. Yield: 244 mg (77%). R_f: 0.52 (EtOAc/hexane, 3 : 7 v/v). IR (ATR): ν = 2982, 1735, 1581, 1446, 1372, 1296, 1238, 1148, 1028, 942, 780, 688, 595 cm^{-1}. ^{1}H NMR (400 MHz, $CDCl_3$): δ 7.57 (d, J = 7.2 Hz, 2H), 7.45 (t, J = 7.6 Hz, 2H), 7.39 (t, J = 7.2 Hz, 1H), 4.88 (s, 1H), 4.28–4.22 (m, 4H), 2.54 (s, 3H), 1.26 (t, J = 7.0 Hz, 6H) ppm. ^{13}C{^{1}H}NMR (100 MHz, $CDCl_3$) δ 166.9, 160.3, 148.4, 128.9, 128.7, 127.9, 127.7, 126.4, 62.1, 50.7, 14.1, 13.9 ppm.

Diethyl 2-[2-methyl-5-(*p*-tolyl)oxazol-4-yl]malonate (3b). Yellow oil. Yield: 239 mg (72%). R_f: 0.55 (EtOAc/hexane, 3 : 7 v/v). IR (ATR): ν = 2995, 2699, 2307, 1736, 1584, 1508, 1373, 1267, 1151, 1094, 1032, 822, 755, 599 cm^{-1}. ^{1}H NMR (400 MHz, $CDCl_3$): δ 7.47 (d, J = 8.0 Hz, 2H), 7.27 (d, J = 8.0 Hz, 2H), 4.87 (s, 1H), 4.29–4.24 (m, 4H), 2.54 (s, 3H), 2.41 (s, 3H), 1.28 (t, J = 7.2 Hz, 6H) ppm. ^{13}C{^{1}H}NMR (100 MHz, $CDCl_3$) δ 167.0, 160.1, 148.5, 138.8, 129.6, 127.2, 126.4, 125.1, 62.1, 50.7, 21.3, 14.1, 14.0 ppm. HRMS (ESI-QTOF) m/z: $[M + H]^+$ calcd for $C_{18}H_{21}NO_5$, 332.1492; found, 332.1506.

Diethyl 2-[5-(4-methoxyphenyl)-2-methyloxazol-4-yl] malonate (3c).[24b] Yellow oil. Yield: 295 mg (85%). R_f: 0.60 (EtOAc/hexane, 2 : 3 v/v). IR (ATR): ν = 1975, 1728, 1588, 1509, 1297, 1240, 1154, 1024, 839, 778, 723, 607 cm^{-1}. ^{1}H NMR (400 MHz, $CDCl_3$): δ 7.51 (d, J = 8.4 Hz, 2H), 6.99 (d, J = 8.8 Hz, 2H), 4.84 (s, 1H), 4.29–4.23 (m, 4H), 3.87 (s, 3H), 2.54 (s, 3H), 1.28 (t, J = 7.2 Hz, 6H) ppm. ^{13}C{^{1}H}NMR (100 MHz, $CDCl_3$) δ 167.1, 159.9, 159.8, 148.4, 128.1, 126.6, 120.5, 114.3 62.1, 55.4, 50.7, 14.1, 14.0 ppm.

Diethyl 2-[5-(4-chlorophenyl)-2-methyloxazol-4-yl]malonate (3d).[24b] Yellow oil. Yield: 257 mg (73%). R_f: 0.57 (EtOAc/

hexane, 3 : 7 v/v). IR (ATR): ν = 2985, 2355, 1737, 1580, 1318, 1241, 1161, 1065, 1026, 947, 844, 679, 597 cm^{-1}. ^1H NMR (400 MHz, $CDCl_3$): δ 7.51 (d, J = 8.8 Hz, 2H), 7.40 (d, J = 8.4 Hz, 2H), 4.83 (s, 1H), 4.27–4.21 (m, 4H), 2.52 (s, 3H), 1.25 (t, J = 7.2 Hz, 6H) ppm. $^{13}C\{^1H\}$NMR (100 MHz, $CDCl_3$) δ 166.8, 160.5, 147.3, 134.7, 129.1, 128.2, 127.6, 126.4, 62.2, 50.8, 14.0, 13.9 ppm.

Diethyl 2-{2-methyl-5-[4-(trifluoromethyl)phenyl]oxazol-4-yl} malonate (3e). Yellow oil. Yield: 308 mg (80%). R_f: 0.63 (EtOAc/hexane, 3 : 7 v/v). IR (ATR): ν = 2995, 2699, 1737, 1585, 1483, 1373, 1267, 1152, 1095, 1031, 942, 834, 755, 598 cm^{-1}. ^1H NMR (400 MHz, $CDCl_3$): δ 7.66 (s, 4H), 4.85 (s, 1H), 4.24–4.18 (m, 4H), 2.50 (s, 3H), 1.21 (t, J = 7.2 Hz, 6H) ppm. $^{13}C\{^1H\}$ NMR (100 MHz, $CDCl_3$) δ 166.6, 161.0, 146.8, 131.2, 129.5, 126.4, 125.8, 125.7, 62.2, 50.9, 13.9, 13.8 ppm. HRMS (ESI-QTOF) m/z: $[M + H]^+$ calcd for $C_{18}H_{18}F_3NO_5$, 386.1210; found, 386.1216.

Diethyl 2-[2-methyl-5-(thiophen-2-yl)oxazol-4-yl]malonate (3f). Brown oil. Yield: 246 mg (76%). R_f: 0.52 (EtOAc/hexane, 3 : 7 v/v). IR (ATR): ν = 3100, 2980, 2360, 1736, 1657, 1580, 1444, 1368, 1235, 1151, 1028, 846, 708, 592 cm^{-1}. ^1H NMR (400 MHz, $CDCl_3$): δ 7.40 (d, J = 4.8 Hz, 1H), 7.29 (d, J = 4.0 Hz, 1H), 7.11 (d, J = 4.4 Hz, 1H), 4.89 (s, 1H), 4.30–4.24 (m, 4H), 2.53 (s, 3H), 1.29 (t, J = 7.2 Hz, 6H) ppm. $^{13}C\{^1H\}$NMR (100 MHz, $CDCl_3$) δ 166.7, 160.2, 143.8, 128.9, 127.8, 127.6, 126.6, 125.9, 62.2, 50.6, 14.1, 14.0 ppm. HRMS (ESI-QTOF) m/z: $[M + H]^+$ calcd for $C_{15}H_{17}NO_5S$, 324.0900; found, 324.0911.

Diethyl 2-[5-(2-butoxyphenyl)-2-phenyloxazol-4-yl]malonate (3g). Yellow oil. Yield: 384 mg (85%). R_f: 0.63 (EtOAc/hexane, 3 : 7 v/v). IR (ATR): ν = 3058, 2967, 2353, 1739, 1587, 1486, 1452, 1371, 1258, 1154, 1031, 1258, 1154, 1031,894, 734, 609 cm^{-1}. ^1H NMR (400 MHz, $CDCl_3$): δ 8.45–8.12 (m, 2H), 7.62–7.60 (m, 1H), 7.49–7.39 (m, 4H), 7.10–7.06 (m, 1H), 7.03 (d, J = 8.4 Hz, 1H), 5.05 (s, 1H), 4.29–4.20 (m, 4H), 4.07 (t, J = 7.0 Hz, 2H), 1.83–1.76 (m, 2H), 1.51–1.41 (m, 2H), 1.29 (t, J = 7.2 Hz, 6H), 0.95 (t, J = 7.4 Hz, 3H) ppm. $^{13}C\{^1H\}$NMR (100 MHz, $CDCl_3$) δ 167.3, 160.5, 156.2, 146.0, 131.2, 130.8, 130.6, 130.2, 128.6, 127.5, 126.6, 120.7, 117.4, 112.4, 68.6, 61.8, 51.4, 30.9, 19.2, 14.0, 13.8 ppm. HRMS (ESI-QTOF) m/z: $[M + H]^+$ calcd for $C_{26}H_{29}NO_6$, 452.2068; found, 452.2078.

Diethyl 2-{5-[2-(2-methoxyethoxy)phenyl]-2-phenyloxazol-4-yl}malonate (3h). Reddish brown oil. Yield: 417 mg (92%). R_f: 0.69 (EtOAc/hexane, 2 : 3 v/v). IR (ATR): ν = 2993, 2299, 1737, 1583, 1486, 1450, 1366, 1268, 1150, 1029, 927, 856, 756, 608 cm^{-1}. ^1H NMR (400 MHz, $CDCl_3$): δ 8.13–8.12 (m, 2H), 7.64–7.62 (m, 1H), 7.47–7.45 (m, 3H), 7.43–7.38 (m, 1H), 7.10 (t, J = 7.6 Hz, 1H), 7.05 (d, J = 8.4 Hz, 1H), 5.22 (s, 1H), 4.29–4.21 (m, 6H), 3.76 (t, J = 5.0 Hz, 2H), 3.40 (s, 3H), 1.29 (t, J = 7.0 Hz, 6H) ppm. $^{13}C\{^1H\}$NMR (100 MHz, $CDCl_3$) δ 167.4, 160.5, 155.7, 145.7, 131.5, 130.7, 130.5, 130.2, 128.6, 127.6, 126.5, 121.2, 117.7, 112.7, 70.6, 68.2, 61.7, 59.1, 51.3, 14.0 ppm. HRMS (ESI-QTOF) m/z: $[M + H]^+$ calcd for $C_{25}H_{27}NO_7$, 454.1860; found, 454.1870.

Diethyl 2-[5-(4-butoxyphenyl)-2-phenyloxazol-4-yl]malonate (3i). Yellow solid. Mp: 80–82 °C. Yield: 370 mg (82%). R_f: 0.63 (EtOAc/hexane, 3 : 7 v/v). IR (ATR): ν = 2931, 1732, 1505, 1303, 1235, 1175, 1031, 789, 701 cm^{-1}. ^1H NMR (400 MHz, $CDCl_3$): δ 8.15–8.12 (m, 2H), 7.62 (d, J = 8.8 Hz, 2H), 7.49–7.48 (m, 3H), 7.02 (d, J = 8.8 Hz, 2H), 4.98 (s, 1H), 4.31–7.24 (m, 4H), 4.05 (t, J = 6.4 Hz, 2H), 1.87–1.80 (m, 2H), 1.59–1.51 (m, 2H), 1.29 (t, J = 7.2 Hz, 6H), 1.03 (t, J = 7.4 Hz, 3H) ppm. $^{13}C\{^1H\}$NMR (100 MHz, $CDCl_3$) δ 167.1, 159.8, 159.6, 148.6, 130.3, 128.7, 128.2, 128.16, 127.3, 126.5, 120.2, 114.8, 67.9, 62.1, 51.3, 31.2, 19.3, 14.0, 13.9 ppm. HRMS (ESI-QTOF) m/z: $[M + H]^+$ calcd for $C_{26}H_{29}NO_6$, 452.2068; found, 452.2077.

Diethyl 2-{5-[2,4-bis(2-methoxyethoxy)phenyl]-2-phenyloxazol-4-yl}malonate (3j). Yellow oil. Yield: 443 mg (84%). R_f: 0.45 (EtOAc/hexane, 2 : 3 v/v). IR (ATR): ν = 2994, 2886, 2699, 1737, 1598, 1455, 1369, 1268, 1185, 1122, 1031, 916, 858, 755 cm^{-1}. ^1H NMR (400 MHz, $CDCl_3$): δ 8.11–8.09 (m, 2H), 7.51 (d, J = 8.4 Hz, 1H), 7.45–7.44 (m, 3H), 6.66–6.62 (m, 2H), 5.14 (s, 1H), 4.26–7.18 (m, 8H), 3.81–3.79 (m, 2H), 3.75–3.73 (m, 2H), 3.49 (s, 3H), 3.39 (s, 3H), 1.28 (t, J = 7.2 Hz, 6H) ppm. $^{13}C\{^1H\}$ NMR (100 MHz, $CDCl_3$) δ 167.5, 161.0, 160.2, 157.0, 145.9, 131.3, 130.5, 130.0, 128.6, 127.6, 126.5, 110.6, 105.9, 70.9, 70.5, 68.2, 67.5, 61.7, 59.3, 59.1, 51.2, 14.0 ppm. HRMS (ESI-QTOF) m/z: $[M + H]^+$ calcd for $C_{28}H_{33}NO_9$, 528.2228; found, 528.2241.

Materials and methods for *in silico* studies

Data set. All the computational studies were performed in the Linux centos-v7.0 platform at the interface of Intel core™ i7-4470 CPU@3.40 GHz processor. Beyond with these specifications, the Auto Dock Vina software was used for molecular docking analysis. The Schrodinger, LLC, New York, 2018-4 software in-built with Qikprop suite was used for ADME (absorption, distribution, metabolism, and excretion) prediction of the AQP4 protein–ligand complexes.[35,36]

Protein structure dataset. As a target of the study, the three-dimensional (3D) structure of AQP4 (PDB-ID: 3gd8) was obtained from the RCSB protein data bank (https://www.rcsb.org).[35,36] Co-crystallized ligands, water molecules, metal ions, cofactors, as well as some missing side chains, incorrect charges, and faulty bond ordering, are frequently found in PDB structures; which were normalized using edit toolbars to add polar hydrogen and charges in order to achieve the appropriate structure. The receptor was then saved in PDBQT format using the Auto Dock Vina protein preparation package.[35,36]

Ligand preparation. The synthesized oxazole derivatives were chosen as ligands for 3D conversion and minimization. All ligand molecules were converted to sdf format, pre-processed with the Auto dock tool and saved in PDBQT format.

Molecular docking analysis. The oxazole derivatives were subjected to molecular docking analysis with Human AQP4 receptor. Using Auto Dock Vina, the receptors were fully prepared. Each protein chain's structure was created by excluding both solvent molecules and receptor-associated binding compounds. The structure of the active site was visualized and predicted using PyMOL software. Based on the active site residues, the grid was generated. The virtual screening of compounds generated as ligands against constructed protein receptors was done using AutoDockVina. The calculated binding energies of the ligands are listed in Table 2.[36–38]

ADME prediction. QikProp is a rapid and accurate prediction programme included in the Schrödinger suite and predicts physically significant descriptors and pharmaceutically relevant features of organic compounds in batches or individually. Qikprop was run in fast mode to predict principle descriptors and ADME properties for all synthesized compounds, including a thorough investigation of QplogBB (blood–brain partition coefficient), QPPCaco (cell line permeability), LogP (octanol/water), HOA% (human oral absorption) and QPPMDCK (MDCK cell permeability). Violation of Lipinski's rule of five was also analyzed.[39,40]

Materials and methods for *in vitro* studies

Chemicals. Chemicals and cell culture reagents were purchased from HiMedia Laboratories Pvt. Ltd, Mumbai, India, Sigma Chemicals Company, Saint Louis, MO, USA, and Sisco Research Laboratories Pvt. Ltd, Mumbai, India.

Cell culture. NCI-H460 cell line was procured from National Centre for Cell Science (NCCS), Pune, India. The cells were cultured in a humidified atmosphere containing 5% CO_2 in a complete medium composed of Dulbecco's Modified Eagle Medium (DMEM), high glucose; supplemented with 4.5 g glucose per litre, 25 mM HEPES, L-glutamine, sodium pyruvate, sodium carbonate, 100 U per mL penicillin, 100 mg per mL streptomycin, and 10% fetal bovine serum. To induce inflammation, cells were treated with LPS for 48 h. The experimental groups includes control, cells treated with LPS (30 μg, 48 h), cells treated with compound **3a** (60 μM, 24 h) and cells pre-treated with compound **3a** (60 μM, 24 h) then with LPS (30 μg, 48 h).

Assay of cell viability. Cell viability was analyzed colorimetrically using 3-(4,5-dimethylthiazol-2-yl)-2,5-diphenyltetrazolium bromide (MTT). Briefly, NCI-H460 [H460] cells were cultured in serum free media either with different concentrations of LPS for 48 h or compound **3a** for 24 h and then MTT solution was added (0.5 mg mL^{-1}) to the cells and incubated for 3–4 h. The blue formazan formed were dissolved in DMSO and the absorbance was read at 550 nm in an ELISA iMARKTM microplate reader (Bio-Rad, USA).

Hemolytic assay. 2 mL of fresh blood was collected in anti-coagulant solution (EDTA tube) from a volunteer with written informed consent, as per the norms of institute ethical committee for human research of Bharathidasan University, constituted based on national ethical guidelines for biomedical and health research involving human participants given by Indian Council of Medical Research, Government of India. Then the blood was centrifuged at 1200*g* for 10 min at 4 °C. Both buffy coat and plasma were discarded. The pellet containing RBC was washed with 20 mM (pH 7) PBS for 5 times. Extent of hemolysis was studied by incubating the RBC suspension with different concentrations of **3a** at room temperature for 4 h. For this assay, Triton X-100 (0.1%) was used as the positive control and phosphate-buffered saline (PBS) was used as the negative control. The suspension was vortexed and centrifuged at 10 000 rpm for 3 min. The supernatant was collected and the optical density (OD) value was observed at 595 nm. The percentage of hemolysis was calculated as follows: % of hemolysis = (OD(test) − OD(negative control))/(OD(positive control) − OD(negative control)) × 100%.

Determination of the gene expression by reverse transcriptase polymerase chain reaction (RT-PCR). The total RNA from NCI-H460 [H460] treated cells were extracted using RNA isolation kit (one step RNA TRIzol reagent; Biobasic Inc., Canada). RT-PCR was carried out with total RNA using iScript cDNA synthesis kit (BioRad, India). The real-time amplification of the cDNA was carried out using SSO Advanced Universal SYBR Green Supermix according to the manufacturer's protocol (Bio-Rad Laboratories, Inc., USA). The Insta Q96 Himedia Real-Time PCR (RT-PCR) (Hi-media, Laboratories Pvt. Ltd, Mumbai, India) was used to analyze the gene expression with specific sets of primers as shown in Table 4. Fold differences in target gene expressions were calculated using the formula $2^{-\Delta\Delta Ct}$. The expressions of the target genes were normalized with internal controls.

Determination of protein expression by western blotting. Protein content of the tissue fractions was estimated by the method of Lowry *et al.* Proteins from cell extracts were separated by SDS-PAGE and subsequently electroblotted onto nitrocellulose membranes. Membranes were blocked for 1 h at room

Table 5 Primary and secondary antibodies used for western blotting

Antibody	Catalogue no.
Aquaporin-4[a]	ABM0022
COX-2[a]	ABP50160
β-actin (13E5)[b]	4970
Secondary anti-mouse IgG[c]	ab97020
Secondary anti-rabbit IgG[c]	ab6722

[a] Abbkine, Inc., China. [b] Cell Signaling Technology, USA. [c] Abcam, Cambridge, UK.

Table 4 Primer sequences for the genes

Gene	Forward primer	Reverse primer
COX-2	CCGGGTACAATCGCACTTAT	GGCGCTCAGCCATACAG
TNFα	CCCAGGGACCTCTCTCTAATCA	AGCTGCCCCTCAGCTTGAG
IL-1β	ACAGATGAAGTGCTCCTTCCA	GTCGGAGATTCGTAGCTGGAT
IL-6	GGTACATCCTCGACGGCATCT	GTGCCTCTTTGCTGCTTTCAC
IL-8	GGCACAAACTTTCAGAGACAGCAG	GTTTCTTCCTGGCTCTT GTCCTAG
IL-10	GGTTGCCAAGCCTTGTCTGA	AGGGAGTTCACATGCGCCT
β-Actin	CGGGAAATCGTGCGTGAC	CGGGAAATCGTGCGTGAC

temperature in 1× TTBS (20 mMTris, pH 7.4; 150 mMNaCl; 0.1% Triton X-100) supplemented with 5% non-fat dry milk. After blotting, membranes were incubated overnight at 4 °C, with specific primary antibodies as shown in Table 5. Membranes were washed four times for 10 min in TTBS and subsequently incubated for 3 h at room temperature with a secondary alkaline phosphatase-conjugated antibody and the proteins were visualized using 5-bromo-4-chloro-3-indolyl phosphate (BCIP/NBT) chromogen substrate (Sigma Chemicals Company, Saint Louis, MO Inc., USA). The densitometric analyses were carried out with lab image platform ver 2.1 software by Kapelan Bio-Imaging GmbH. The expression of each target proteins was normalized with corresponding internal controls.

Data analysis

The values are expressed as mean ± standard deviation (SD). Differences between the groups were assessed by one-way ANOVA using GraphPad Prism 9.0 software. Post hoc testing was performed for inter-group comparisons using Tukey's multiple comparisons test. Values were considered significant at $P < 0.05$. $^{**}P < 0.01$ and $^{***}P < 0.001$.

Conflicts of interest

There are no conflicts to declare.

Acknowledgements

The authors thank Tamil Nadu State Council for Higher Education (TANSCHE) for financial support and DST-FIST for infrastructure/instrumentation facilities at Bharathidasan University. K. S. also thanks Council of Scientific and Industrial Research (CSIR), India for financial support. T. S. thanks Department of Science and Technology (DST) for a WOS-A fellowship.

Notes and references

1 (*a*) B. Moldoveanu, P. Otmishi, P. Jani, J. Walker, X. Sarmiento, J. Guardiola, M. Saad and J. Yu, *J. Inflammation Res.*, 2009, **2**, 1–11; (*b*) M. Antonelli and I. Kushner, *FASEF J.*, 2017, **31**, 1787–1797; (*c*) M.-G. Netea, F. Balkwill, M. Chonchol, F. Cominelli, M.-Y. Donath, G. Bourboulis, D. Golenbock, M.-S. Gresnigt, M.-T. Heneka, H.-M. Hoffman, R. Hotchkiss, A.-B. Joosten, D.-L. Kastner, M. Korte, E. Latz, P. Libby, T.-M. Poulsen, A. Mantovani, H.-G. Mills, K.-L. Nowak, L.-A. O'Neill, P. Pickkers, T.-V. Poll, P.-M. Ridker, J. Schalkwijk, D.-A. Schwartz, B. Siegmund, C.-J. Steer, H. Tilg, W.-M. Meer, F.-L. Veerdonk and C.-A. Dinarello, *Nat. Immunol.*, 2017, **18**, 826–832; (*d*) D.-R. Germolec, K.-A. Shipkowski, R.-P. Frawley and E. Evans, *Methods Mol. Biol.*, 2018, **1803**, 57–79; (*e*) J.-M. Zhang and J. An, *Int. Anesthesiol. Clin.*, 2007, **45**, 27–37.

2 B. Hu, S. Huang and L. Yin, *J. Med. Virol.*, 2021, **93**, 250–256.

3 (*a*) C. Pelaia, C. Tinello, A. Vatrella, G.-D. Sarro and G. Pelaia, *Ther. Adv. Respir. Dis.*, 2020, **14**, 1–19; (*b*) C. Peteranderl, J.-I. Sznajder, S. Herold and E. Lecuona, *Front. Immunol.*, 2017, **8**, 446–456.

4 G. Benga, *Mol. Aspects Med.*, 2012, **33**, 514–517.

5 (*a*) M.-C. Papadapoulos, S. Saadoun and A. S. Verkman, *Pflügers Archiv: European Journal of Physiology*, 2008, **456**, 693–700; (*b*) M.-C. Papadopoulos and S. Saadoun, *Biochimica et Biophysica*, 2015, **1848**, 2576–2583; (*c*) S. Edamana, F.-H. Login, S. Yamada, T.-H. Kwon and L.-N. Nejsum, *Am. J. Physiol.: Cell Physiol.*, 2021, **320**, 771–777.

6 H. Lv, Y. Li, C. Xue, N. Dang, C. Bi and A. Shan, *J. Anim. Physiol. Anim. Nutr.*, 2022, **106**, 167–180.

7 (*a*) G. Tang and G.-Y. Yang, *Int. J. Mol. Sci.*, 2016, **17**, 1413–1424; (*b*) A.-M. Fukuda and J. Badaut, *J. Neuroinflammation*, 2012, **9**, 279–288.

8 (*a*) A.-S. Verkman, J. Ratelade, A. Rossi, H. Zhang and L. Tradtrantip, *Acta Pharmacol. Sin.*, 2011, **32**, 702–710; (*b*) Y.-L. Lan, D.-Y. Fang, J. Zhao, T.-H. Ma and S. Li, *Acta Neurol. Belg.*, 2016, **116**, 127–134; (*c*) H.-I. Kataoka, *Int. J. Mol. Sci.*, 2016, **17**, 1306–1322.

9 S. Liu, J. Mao, T. Wang and X. Fu, *Mol. Neurobiol.*, 2017, **54**, 6426–6435.

10 (*a*) A.-S. Verkman, *Respir. Physiol. Neurobiol.*, 2007, **159**, 324–330; (*b*) A. Zannetti, G. Benga, A. Brunetti, F. Napolitano, L. Avallone and A. Pelagalli, *Cells*, 2020, **9**, 2678–2695.

11 (*a*) Z. Borok and A.-S. Verkman, *J. Appl. Physiol.*, 2002, **93**, 2199–2206; (*b*) R. Meli, C. Pirozzi and A. Pelagalli, *Front. Physiol.*, 2018, **9**, 101–112; (*c*) D. Vecchio, C. Solaro, E. Virgilio, P. Naldi, R. Bottero, F. Masuccio, M. Capabianco and R. Cantello, *Sclerosis*, 2023, **1**, 1–4.

12 (*a*) E. Yadav, N. Yadav, A. Hus and J.-S. Yadav, *Respir. Med.*, 2020, **174**, 106193–106210; (*b*) I.-V. da Silva and G. Soveral, *Int. J. Mol. Sci.*, 2021, **22**, 1845–1860.

13 C. Guo, T. Wu, H. Zhu and L. Gao, *Inflammation*, 2019, **42**, 1401–1412.

14 M.-M. Salman, P. Kitchen, A.-J. Yool and R.-M. Bill, *Trends Pharmacol. Sci.*, 2022, **43**, 30–42.

15 L. Tradtrantip, B.-J. Jin, X. Yao, M.-O. Anderson and A.-S. Verkman, *Adv. Exp. Med. Biol.*, 2017, **967**, 239–250.

16 A.-S. Verkman, A.-J. Smith, P.-W. Phuan, L. Tradtrantip and M.-O. Anderson, *Expert Opin. Ther. Targets*, 2017, **21**, 1161–1170.

17 F.-J.-M. Detmers, B.-L. de-Groot, E.-M. Muller, A. Hinton, I.-B.-M. Konings, M. Sze, S.-L. Filtsch, H. Grubmuller and P.-M.-T. Deen, *J. Biol. Chem.*, 2006, **281**, 14207–14214.

18 M.-A. Awan, P. Kitchen, M.-M. Salman, M.-T. Conner, A.-C. Conner and R.-M. Bill, *Int. J. Mol. Sci.*, 2009, **20**, 1589–1608.

19 V.-J. Huber, M. Tsujita, M. Yamazaki, K. Sakimura and T. Nakada, *Bioorg. Med. Chem. Lett.*, 2007, **17**, 1270–1273.

20 I. Pirici, T.-A. Balsanu, C. Bogdan, C. Margaritescu, T. Divan, V. Vitalie, L. Magoanta, D. Pirici, R.-O. Carare and D.-F. Muresanu, *Int. J. Mol. Sci.*, 2018, **19**, 46–64.

21 N. Azh, F. Barzkar, N.-M. Gorji, P.-P. Talatappeh, Y. Moradi, R.-V. Azad, M. Ranjbar and H.-R. Baradaran, *Pharmacol. Res. Perspect.*, 2022, **10**, 925–956.

22 (*a*) J.-T. Mhlongo, E. Brasil, B.-G. Torre and F. Albericio, *Mar. Drugs*, 2020, **18**, 203–228; (*b*) Z. Jin, *Nat. Prod. Rep.*, 2011, **28**, 1143–1191.

23 (*a*) H.-Z. Zhang, Z.-L. Zhao and C.-H. Zhou, *Eur. J. Med. Chem.*, 2018, **144**, 444–492; (*b*) R. Kuand, H.-J. Shue, D.-J. Blythin, N.-Y. Shih, D. Gu, X. Chen, J. Schwerdt, L. Lin, P.-C. Ting, X. Zhu, R. Aslanian, J.-J. Piwinski, L. Xiao, D. Prelusky, P. Wu, J. Zhang, X. Zhang, C.-S. Celly, M. Minnicozzi, M. Billah and P. Wang, *Bioorg. Med. Chem. Lett.*, 2007, **17**, 5150–5154; (*c*) H.-R. Chobanian, Y. Guo, P. Liu, M.-D. Chioda, S. Fung, T.-J. Lanza, L. Chang, R.-K. Bakshi, J.-P. Dellureficio, Q. Hong, M. McLaughlin, K.-M. Belyk, S.-W. Krska, A.-K. Makarewicz, E.-J. Martel, J.-F. Leone, L. Frey, B. Karanam, M. Maderia, R. Alvaro, J. Shuman, G. Salituro, J.-L. Terebetski, N. Jochnowitz, S. Mistry, E. McGowan, R. Hajdu, M. Rosenbach, C. Abbadie, J.-P. Alexander, L.-L. Shiao, K.-M. Sullivan, R.-P. Nargund, M.-J. Wyvratt, L.-S. Lin and R.-J. DeVita, *ACS Med. Chem. Lett.*, 2014, **5**, 717–721; (*d*) D. Zhang, J. Guo, M. Zhang, X. Liu, M. Ba, X. Tao, L. Yu, Y. Guo and J. Dai, *J. Nat. Prod.*, 2017, **80**, 3241–3246; (*e*) N.-C. Desai, D.-V. Vaja, S.-B. Joshi and V.-M. Khedkar, *Res. Chem. Intermed.*, 2021, **47**, 573–587; (*f*) N.-Y. Pepinosa, M.-G. Trujillo, S.-C. Castano, L.-A. Veloza and J.-C. Arias, *Biomed. Pharmacother.*, 2021, **138**, 111495–111510; (*g*) H. Ahmad, S. Ullah, F. Rahman, A. Saeed, J. Pelletier, J. Sevigny, A. Hassan and J. Iqbal, *Eur. J. Med. Chem.*, 2020, **208**, 112759–112768; (*h*) C. Maria, L. Gluseppe, C. Ugo, G. Salvatore, R. Roberto, I. Daniela and L. Laura, *Curr. Med. Chem.*, 2019, **26**, 7337–7371.

24 (*a*) T. Selvi and K. Srinivasan, *J. Org. Chem.*, 2014, **79**, 3653–3658; (*b*) T. Selvi and K. Srinivasan, *Chem. Commun.*, 2014, **50**, 10845–10848; (*c*) M. Meenakshi and K. Srinivasan, *Org. Biomol. Chem.*, 2022, **20**, 8741–8746.

25 M. Meenakshi, P. Antojenifer, M. Karthikeyan, C. Prahalathan and K. Srinivasan, *J. Heterocycl. Chem.*, 2022, **59**, 351–358.

26 (*a*) L.-F. M. Antony, A. Kannan, A. Panneerselvam, C. Loganathan, E.-M. Shankar, K. Anbarasu and C. Prahalathan, *Inflammation*, 2020, **43**, 1599–1609; (*b*) L.-F. M. Antony, A. Kannan, A. Panneerselvam, C. Loganathan, K. Anbarasu and C. Prahalathan, *Med. Hypotheses*, 2020, **143**, 110201–110206.

27 S. Liu, J. Mao, T. Wang and X. Fu, *Mol. Neurobiol.*, 2017, **54**, 6426–6435.

28 L. Li, H. Zhang, M.-V. Doyer, S.-S. Zamvil and A.-S. Verkman, *FASEB J.*, 2011, **25**, 1556–1566.

29 W. Dai, J. Yan, G. Chen, G. Hu, X. Zhou and X. Zeng, *Int. J. Mol. Med.*, 2018, **42**, 1716–1722.

30 F. Zhao, J. Deng, X. Xu, F. Cao, K. Lu, D. Li, X. Cheng, X. Wang and Y. Zhao, *J. Neuroinflammation*, 2018, **15**, 157–170.

31 D.-K. Binder, K. Oshio, T. Ma, A.-S. Verkman and G. Manley, *NeuroReport*, 2004, **15**, 259–262.

32 Y. Dunder, S. Unlu, E. Banoglu, A. Entrena, G. Costantino, M.-T. Nunez, F. Ledo, M.-F. Sahin and N. Noyanalpan, *Eur. J. Med. Chem.*, 2009, **44**, 1830–1837.

33 H.-R. Chobanian, Y. Guo, P. Liu, M.-D. Chioda, S. Fung, T.-J. Lanza, L. Chang, R.-K. Bakshi, J.-P. Dellureficio, Q. Hong, M. McLaughlin, K.-M. Belyk, S.-W. Krska, A.-K. Makarewicz, E.-J. Martel, J.-F. Leone, L. Frey, B. Karanam, M. Madeira, R. Alvaro, J. Shuman, G. Salituro, J.-L. Terebetski, N. Jochnowitz, S. Mistry, E. McGowan, R. Hajdu, M. Rosenbach, C. Abbadie, J.-P. Alexander, L.-L. Shiao, K.-M. Sullivian, R.-P. Nargund, M.-J. Wyvratt, L.-S. Lin and R.-J. DeVita, *ACS Med. Chem. Lett.*, 2014, **5**, 717–721.

34 K. Seth, S.-K. Garg, R. Kumar, P. Purohit, V.-S. Meena, R. Goyal, U.-C. Banerjee and A.-K. Chakraborti, *ACS Med. Chem. Lett.*, 2014, **5**, 512–516.

35 L. Loganathan, K. Muthusamy, J.-M. Jayaraj, A. Kajamaideen and J.-J. Balthasar, *J. Biomol. Struct. Dyn.*, 2018, **37**, 3637–3648.

36 Q. Xue, X. Liu, P. Russell, J. Li, W. Pan, J. Fu and A. Zhang, *Ecotoxicol. Environ. Saf.*, 2022, **233**, 113323.

37 A. Markou, L. Unger, M. Abir-Awan, A. Saadallah, A. Halsey, Z. Balklava, M. Conner, S. T Horsefield, S.-D. Greenhill, A. Conner and R.-M. Bill, *Biochim. Biophys. Acta, Biomembr.*, 2022, **1864**, 183853.

38 Y. Abe and M. Yasui, *Biomolecules*, 2022, **12**, 591.

39 *Schrödinger Release 2020-1*, qikprop Schrödinger, LLC, New York, NY, 2020.

40 J.-M. Jayaraj, M. Jothimani, C.-P. Palanisamy, O.-T. Pentikäinen, M. Pannipara, A.-G. Al-Sehemi, K. Muthusamy and K. Gopinath, *Bioinorg. Chem. Appl.*, 2022, 8635054.